Inhibition of KRAS codon 12 mutants using a novel DNA-alkylating pyrrole-imidazole polyamide conjugate

Kiriko Hiraoka[1], Takahiro Inoue[1], Rhys Dylan Taylor[2], Takayoshi Watanabe[1], Nobuko Koshikawa[1], Hiroyuki Yoda[1], Ken-ichi Shinohara[1], Atsushi Takatori[1], Kazuhiro Sugimoto[3], Yoshiaki Maru[1], Tadamichi Denda[4], Kyoko Fujiwara[5], Allan Balmain[6], Toshinori Ozaki[3], Toshikazu Bando[2], Hiroshi Sugiyama[2], and Hiroki Nagase[1]

Authors' Affiliations: [1]Laboratory of Cancer Genetics, Chiba Cancer Center Research Institute, 666-2 Nitona, Chuoh-ku, Chiba 260-8717, Japan; [2]Department of Chemistry, Graduate School of Science, Kyoto University, Kitashirakawa-oiwakecho, Sakyo-ku, Kyoto 606-8502 Japan [3]Laboratory of DNA Damage Signaling, Chiba Cancer Center Research Institute, 666-2 Nitona, Chuoh-ku, Chiba 260-8717, Japan; [4]Department of Gastroenterology, Chiba Cancer Center, 666-2 Nitona, Chuoh-ku, Chiba 260-8717, Japan [5]Innovative Therapy Research Group, Nihon University Research Institute of Medical Science, Nihon University School of Medicine, 30-1 Ooyaguchi-kami, Itabashi-ku, Tokyo 173-8610, Japan. [6] Helen Diller Family Comprehensive Cancer Center, University of California, San Francisco, CA 94158

Correspondence: H.N. (hnagase@chiba-cc.jp)

Abstract

Despite extensive efforts to target mutated RAS proteins, anti-cancer agents capable of selectively killing tumour cells harbouring KRAS mutations have remained unavailable. Here, we demonstrate the direct targeting of *KRAS* mutant DNA using a synthetic alkylating agent (pyrrole-imidazole polyamide indole-*seco*-CBI conjugate; KR12) that selectively recognises oncogenic codon 12 *KRAS* mutations. KR12 alkylates adenine N3 at the target sequence, causing strand cleavage and growth suppression in human colon cancer cells with G12D or G12V mutations, thus inducing senescence and apoptosis. In xenograft models, KR12 infusions induce significant tumour growth suppression, with low host toxicity in *KRAS*-mutated but not wild-type tumours. This newly developed approach may be applicable to the targeting of other mutant driver oncogenes in human tumours.

Recent advances in the next-generation sequencing of human tumours have uncovered hundreds of recurrent oncogenic driver mutations and have identified many novel, actionable therapeutic targets. Oncogenic driver genes, which are often mutated, are continuously expressed and thereby contribute to cancer cell survival, which is a target for clinical therapy. Targeting the RAS-MAPK pathway has led to the development of successful treatments of EGFR-mutant cancers but has also revealed that unexpected degrees of oncogene addiction and signalling complexity exist [14]. A common outcome of treatment using inhibitors of genes that lie "downstream" in the RAS pathway is the development of drug resistance [16], and new approaches that target mutant RAS genes may provide a more direct route to inhibit these poor-prognosis tumours.

RAS genes, particularly H-ras, N-ras, and K-ras, were the first human oncogenes to be discovered in human tumours more than 30 years ago and are among the most commonly mutated and critical cancer driver genes. The legendary K-Ras protein has been on everyone's "target" list since its discovery. It has been estimated that approximately 33,000 newly diagnosed colon cancer patients in the United States during the year 2013 had the *KRAS* (G12D) mutation, which is considered the most frequent mutation in metastatic colon cancer, or the (G12V) mutation [12,19]. Extensive efforts have therefore been made to develop one or more small chemical compounds that could directly target and inhibit constitutively active KRAS. Unfortunately, direct pharmacological targeting of activated KRAS has, to date, been unsuccessful for clinical use [25]. Recently, a G12C KRAS mutation has been successfully targeted *in vitro* by a small molecule that allosterically controls GTP affinity and effector interactions, representing a promising approach to therapy for this specific subset of KRAS mutant tumours [13]. In the face of the challenges in developing small-molecule drugs that directly target *KRAS* mutant proteins [17], we have developed a novel approach that directly targets the mutant DNA. Hairpin pyrrole (Py)-imidazole (Im) (PI) polyamides can be designed to bind with high affinity to the minor groove of specific DNA sequences [6]: Py moieties preferentially bind T, A and C bases, but not G, whereas Im is a G-reader. These agents have shown efficacy in preclinical animal models of human diseases, including cancer, with minimal toxicity [11,21,24]. For example, PI polyamide conjugates with 1,2,9,9a-tetrahydrocyclopropa[1,2-c]benz[1,2-e]indol-4-one (CBI), which is converted to its cyclopropyl form via cyclisation of a precursor containing a chloro-methyl group to alkylate target DNA at the minor groove of N3 of adenine under neutral pH conditions, is a synthetic analogue of the alkylating moiety of duocarmycin A and can improve the limitations of targeting a coding sequence [3,22,23]. We therefore synthesised PI polyamide indole-*seco*-CBI

conjugates to target common KRAS codon 12 mutations.

Results

KR12 targets KRAS codon 12 (G12D and G12V) mutants

The compounds IPβIIPI-γ-PIβPP-indole-*seco*-CBI (KR12: Fig. 1 (a)) and IIPIβPI-γ-PIPβP-indole-*seco*-CBI (#6) [18] were designed and synthesised to recognise and alkylate adenine residues on the template strand of exon 2 of mutant *KRAS*, specifically at codon 12 (GTT and GAT) and codon 13 (GAC), respectively, according to the general recognition rule for PI polyamides [6]. The hairpin PI polyamide for KR12 but not for #6 preferentially bound to the mutant KRAS sequences, compared with wild-type, as shown by gel shift and Surface Plasmon Resonance assays (Supplementary Fig. 1 and 2, and Supplementary Table 1). Alkylation of theoretical recognition sequences, i.e., 5'-WCGCCWWCA-3' for KR12 and 5'-WCGWCWCCA-3' for #6 (W indicates A or T), was confirmed using a thermally induced strand cleavage procedure [18]. Dose-dependent, alkylation-mediated selective DNA strand cleavage was detected at the G12D/G12V mutations in the presence of KR12 (Fig. 1 (b)), and #6 showed specific cleavage of the sequence at the codon 13 mutation [18]. Strong, dose-dependent alkylation by KR12 was detected only at the mutated KRAS codon 12 target sites among approximately 160 base pairs of KRAS EXON2 plus plasmid sequences, which did not have additional full-match recognition sites of KR12.

The KR12-induced cell growth inhibition of a series of KRAS mutated or non-mutated human colon cancer cell lines, i.e., HT29 (WT), Caco-2 (WT), SW1463 (12C/12C; GGT-TGT), SW480 (12V/12V; GGT-GTT), SW620 (12V/12V) and LS180 (12D; GGT-GAT/WT), were then analysed using the standard WST (water soluble tetrazolium salts) assay. The viability of *KRAS* G12D or G12V mutant cells was significantly lower after treatment compared to wild-type cells or SW1463 cells carrying the G12C mutation, which is not recognised by KR12 (Fig. 2 (a)) (see also additional data on cell lines SNU-C2B (12D/12D) and DLD1 (13D/WT) in Supplementary Table. 2). A distinct pattern of cell viability was observed after KR12 treatment. Cell lines with KR12-recognised KRAS mutations (12D or 12V) were more sensitive than cell lines without those sequences, while there was no correlation between cell growth and p53 mutation status.

Mutant KRAS suppression induced by KR12

To analyse the specific alkylation and subsequent downregulation of the KRAS mutant allele after KR12 treatment, human colon cancer-derived, heterozygously mutated LS180 (12V/WT) cells were used to evaluate allele-specific suppression after DMSO, KR12, #6 or KR12 lacking *seco*-CBI (Dp) treatment. Endogenous DNA alkylation at the KRAS codon 12 mutation in LS180 cells after KR12 but not after #6 or DMSO treatment was repeatedly confirmed using ligation-mediated PCR (Supplementary Fig. 3). Unlike DMSO-, #6- or Dp-treated cells, KR12-treated cells showed significant downregulation of total *KRAS* and mutated *KRAS* allele expression by quantitative rtPCR and colony PCR/sequencing assays, respectively (Fig. 2 (b) and (c), and supplementary Table 3). Immunoblot analysis also revealed that KR12, but not #6, induced a significant reduction in KRAS protein levels and in its GST-Raf-bound, active GTP-bound form, whereas KR12 had an undetectable effect on KRAS levels or activity in HT29 cells harbouring wild-type *KRAS* (Fig. 2 (d)). In contrast to KR12, Dp had an undetectable effect on *KRAS* codon 12 mutant expression, indicating that the targeted hairpin PI polyamide lacking the CBI alkylating moiety was not sufficient to reduce the expression of the targeted mutant gene (Fig. 2 (b)). Induction of 12V mutation sequence-specific alkylation after KR12 treatment could induce specific reductions in mutated KRAS RNA and activated KRAS protein levels in heterozygous LS180 cells. We also observed slight reduction of KRAS downstream proteins of phospho-AKT and phospho-ERK expression after KR12 treatment (Supplementary Fig. 4 (d)).

Senescence and DNA damage induced by KR12 in LS180 cells

We next investigated the biological effects of KR12 on *KRAS* mutant colon carcinoma cells. After 48 hours of 100 nM KR12-treatment, a flat cell morphology was displayed in LS180 cells, and SA-β-gal activity was strongly increased compared to DMSO- or #6-treated cells, suggesting that KR12 induced cellular senescence (Fig. 3 (a)). Cellular senescence is a stress response that stably blocks proliferation induced by activation of the RAS pathway, but is dependent on the cellular context [5]. Cell cycle arrest is a critical process in cellular senescence that is induced by the CDK inhibitor $p21^{WAF1/CIP1}$ [4], and 48-hour KR12 exposure significantly increased the proportion of G2/M-phase cells (Fig. 3 (b)). In contrast, DMSO and #6 had less of an effect on cell cycle distribution, and none of the three treatments increased the number of sub-G1-phase cells or the level of apoptotic genomic DNA fragmentation (Fig. 3 (c)). KR12 markedly induced phosphorylation of p53 at Ser-15, $p21^{WAF1/CIP1}$ and phosphorylated histone variant H2AX (γH2AX), whereas KR12-mediated cleavage of PARP at the 48 hour time point was not observed (Fig. 3 (d)). Phospho-p53

(Ser-15) and γH2AX inductions in KR12-treated cells were also visually confirmed by indirect immunofluorescence staining (Supplementary Fig. 4 (b)). We conclude that KR12 promotes p53-dependent cellular senescence, which is an important tumour suppressor mechanism [5], as well as DNA double-strand breaks, but not apoptosis, after short-term treatment.

p53 dependent apoptosis is induced by KR12 in LS180 cells

Strong induction of apoptosis was, however, observed in LS180 cells after fourteen days of continuous 50 nM KR12 treatment, as evidenced by the significant increase in sub-G1-phase cells shown by FACS analysis (Fig. 3 (b) and Supplementary Fig. 4 (a)) and typical DNA fragmentation (Fig. 3 (c)), while #6 induced G2/M arrest. LS180 cells, which carry hemizygous wild-type *p53* [10], showed marked induction of p53 in association with cleaved PARP accumulation and γH2AX, while treatment with #6 resulted in faint p53 activation without PARP cleavage (Fig. 3 (d)), implying that apoptosis induction by long-term KR12 treatment might be p53-dependent. The induction of p53 phosphorylation at Ser-15 and of γH2AX was also visually confirmed by indirect immunofluorescence staining (Supplementary Fig. 4 (c)). Based on these data, we propose that treatment of LS180 cells with KR12, but not with #6, introduces DNA breaks at the KRAS locus and induces γH2AX foci and senescence and that after extended exposure to the drug, apoptosis occurs.

KRAS knockdown enhances DNA alkylator-induced cell death

To confirm a possible synergy of DNA alkylator and KRAS suppression in LS180 cells, we assessed LS180 growth inhibition after treatments with siRNA targeting KRAS, control siRNA, #6 (KRAS non-targeting PI polyamide-indole-secoCBI) and combinations of siRNAs and #6. Although single treatments with either KRAS siRNA or #6 with control siRNA resulted in reduced LS180 cell viability, 1 nM of KRAS siRNA induced a partial reduction of cell growth. When treated together with a low dose (0.3 nM) of #6, 1 nM of KRAS siRNA resulted in significantly higher cell growth reduction than samples treated with 1 nM of control siRNA (Supplementary Fig. 5 (a) and (b)), implying that even partial reduction of KRAS and its downstream signals may sufficiently increase the sensitivity of alkylating agents in LS180 cells. KR12 also caused partial downregulation of the active KRAS mutant and of DNA alkylation induction; therefore, KR12 increases its own ability to induce DNA damage, which is followed by cell death, in a similar manner.

Preferential *in vivo* tumour growth reduction by KR12

The potential efficacy of KR12 *in vivo* was tested by weekly intravenous injection of DMSO or KR12 (320 μg/kg) for 5 weeks into nude mice inoculated with HT29 (KRAS WT), LS180 (heterozygous 12D/WT), or SW480 (homozygous 12V) cells. Treatment was started when the tumour size reached 100 mm^3 (Supplementary Table 4 and Supplementary Fig. 6 (a)). KR12 injection had an undetectable effect on the growth of HT29 tumours, whereas a significant reduction of tumour growth, with minimum toxicity, was demonstrated for the SW480 (P=0.0009) and LS180 (P=0.0122) tumours upon significantly reducing KRAS expression in those tumours (P=0.0388) (Fig. 4 and Supplementary Figs. 6 (b) and 7 (b)). Even after cessation of treatment at 5 weeks, KR12-treated SW480 tumours consistently showed slower growth than the DMSO-treated controls (Supplementary Fig. 7 (a)). Furthermore, the KR12-treated SW480 tumours exhibited movable, hard fibrotic nodules. We also examined the same experiment using an alkylating agent of CBI itself and #6, which should not have performed specific alkylation at the KRAS 12D mutation. Although CBI showed a strong anti-tumour effect, this tumour growth reduction was slightly weaker than that from KR12 treatment, and #6 did not show any significant anti-tumour effects in the SW480 xenografted nude mouse model. It was also intriguing that mice treated with KR12, #6 or DMSO remained healthy during the experiment, while CBI-treated mice exhibited weight loss and slight illness (Supplementary Fig. 7 (a)).

Discussion

Although other drugs have been developed against the RAS signalling pathway, they are mainly effective against cancers with wild-type KRAS and are often ineffective in the treatment of KRAS-mutated colorectal cancers [20]. The PI polyamide-based alkylation strategy specifically downregulated constitutively active KRAS and efficiently suppressed the *in vitro* growth of several KRAS mutant cancer cell lines through the induction of DNA damage and cellular senescence followed by apoptosis. The *in vivo* growth of KRAS G12V/G12D mutant tumour xenografts was also efficiently suppressed by weekly injections of KR12 into mice bearing tumours induced by the inoculation of LS180 or SW480 cells. Therefore, KR12 is a promising anti-cancer drug candidate for unmet KRAS codon 12 mutant cancers. We propose that PI polyamide-mediated-specific silencing of mutant oncogenic driver genes may therefore facilitate the development of a pipeline of next-generation, molecular targeted

therapeutic strategies that could be applied in combination with mutant driver gene identification by sequencing the exomes of human cancers as a route to "Precision Medicine" that is targeted at the individual patient.

Hairpin *N*-methylpyrrole(Py)-*N*-methylimidazole(Im) polyamide indole-*seco*-CBI conjugates [3,22] can be designed for specific 9-base-pair recognition of the genome following Dervan's recognition rule, as seen in natural minor groove binders, which undergo hydrogen bonding to DNA [6]. Under neutral pH, the open-ringed *seco*-CBI moiety is converted to CBI, which then alkylates the N3 of adenine in the DNA minor groove. When conjugated to PI polyamide indole, the conjugates increase sequence recognition specificity compared to conventional alkylating agents, which mainly recognise the N6 of guanine in the DNA major groove without recognising the genomic DNA sequence [2,3,22,23]. Although indole, γ-aminobutyric acid (γ-turn) and beta-alanine linker may require optimisation to improve their specificity and sensitivity for sequence-specific alkylation, the recognition of specific 9-bp sites in the genome by KR12 allows for multiple recognition sites (approximately 9,121 sites in the human genome (GRCh38/hg38)), where the mutated KRAS site should be included for preferential alkylation.

KR12 treatment resulted in a significant reduction of activated KRAS and a significant induction in DNA damage followed by cell death in KRAS-mutated colon cancer cells. We observed dose-dependent alkylation at the mutated sequences by CBI conjugates, with approximately a ten-fold difference in the dissociation constants of the mutant and wild-type allele sequences, a reduction of mutant KRAS expression in heterozygous LS180 cells, endogenous alkylation of the KRAS mutant genome, and *in vitro* and *in vivo* growth reduction of tumour cells with the KRAS mutations. All together, these results suggest that the DNA sequence-specific alkylating activity of hairpin polyamide indole-*seco*-CBI recognises the match sequence instead of the mismatch site. The number of naked PI polyamides showing biological efficacy as single agents remains limited. Thus, one way to enhance the therapeutic potential of PI polyamides might be to conjugate them to small-molecule drugs, such as alkylating agents [7, 8].

In many clinical trials, chemotherapy and targeted therapy combinations result in better outcomes for patients and prolong overall survival. As KR12 is an alkylating agent targeting a restricted number of genomic regions, including the KRAS driver oncogene mutation, it appears suited for combination therapy between molecular targeted therapy and conventional chemotherapy. Because of the sequence-specific DNA recognition of KR12, the number of genomic regions that are alkylated by KR12 should also be dramatically reduced in

comparison to conventional chemotherapy; therefore, the adverse effect of toxicity to normal cells may be remarkably reduced, as demonstrated in animal experiments (Supplementary Fig. 7 (a)). Although potential off-target effects of KR12 should exist among the 9,121 estimated target sites in the reference human genome (GRCh38/hg38), this possibility may not be a major concern for cancer patients with poor prognosis and experience with conventional chemotherapy. Although many issues still remain to be addressed for the clinical development of PI polyamide-indole-seco-CBI, as usually seen in cases of drug development, targeting oncogenic driver genes for alkylation may promise a fruitful feature of cancer therapy for untreatable cancer patients with unfavourable prognoses. Extensive genomic sequencing of tumour and normal tissues may provide critical biomarkers to aid in finding appropriate cancer cases that should be treated by KR12 or another specific genome-targeting alkylator.

Tumour selectivity is another important issue for anti-cancer treatment. In contrast to traditional cytotoxic chemotherapies, which crudely target growth processes shared by normal and cancerous tissues, agents such as Imatinib mesylate (Gleevec) for BCR-ABL translocation that target genetic alterations underlying cancer often have mild toxicity because of their greater specificity for cancer cells [9]. In addition to specificity to the cancer genome, PI polyamide has been reported to accumulate specifically in xenografted tumour tissue in some cases [15]. These unique properties of PI polyamide conjugates provide a very efficient capacity for drug delivery, and its alkylating conjugate, which targets oncogenic somatic mutations, could reveal a superb selective advantage by specifically targeting cancer cells with the mutation. This possibility may also support the observed very specific and effective *in vivo* anti-cancer activity of KR12.

In conclusion, a synthetic PI polyamide alkylator conjugate of KR12 has been designed to target KRAS mutations and induce mutant KRAS suppression followed by tumour cell death *in vitro* and *in vivo* in an oncogenic mutation-specific manner. Thus, KR12 is a possible candidate drug for colorectal patients with either the G12D or G12V mutation.

METHODS

Compounds

The compounds ImPyβImImPyIm-γ-PyImβPyPy-indoleCBI (KR12), shown in Fig. 1 (a), and ImPyβImImPyIm-γ-PyImβPyPy-indoleCBI (#6) [18] were designed and synthesised as

described previously [2]. Briefly, PI polyamides were synthesised in a stepwise reaction using a previously described Fmoc solid-phase protocol [3] and a peptide synthesizer (PSSM-8, Shimadzu Industry) with a computer-assisted operation system on a 10-μmol scale (9.8 mg of Fmoc-β-alanine Wang resin). After synthesis, 1 mL of 50% 1 N LiOH/NMP was mixed with the resin, and the mixture was heated at 55 ºC for 1 hour to detach the PI polyamides from the resin. The PI polyamides were then purified by high-performance liquid chromatography (HPLC) LC-20 (Shimadzu Industry) using a 10 mm x 150 mm Phenomenex Gemini-NX3u 5-ODS-H reverse-phase column in 0.1% acetic acid in water, with acetonitrile as the eluent, a flow rate of 10 mL/min, a linear gradient from 30% to 75% acetonitrile over 30 minutes, and detection at 310 nm. Collected KR12-COOH fractions were analysed by LC-MS. DIEA (0.5 μL, 2.86 μmol) and PyBOP (1.0 mg, 1.95 μmol) were added to a solution of Py–Im polyamide carboxylic acid KR12-COOH (1.0 mg, 0.66 μmol) in NMP (100 μL), and the reaction mixture was stirred for 1 hour at room temperature. After conversion from KR12-COOH to the activated 1-hydroxybenzotriazole ester was verified by analytical HPLC (0.1% TFA/CH3CN 30–75% linear gradient, 0-30 min), NH_2-indole seco-CBI (0.6 mg, 1.58 μmol) was added to the reaction vessel, and the reaction mixture was stirred for 4 days at room temperature. The reaction mixture was subjected to HPLC purification (0.1% TFA/CH3CN 30–75% linear gradient, 0–30 min), and the peak fraction containing the product was collected. After lyophilisation, KR12 was produced as a white powder.

High–resolution gel electrophoresis

5’-Texas Red-labelled DNA fragments containing the indicated *KRAS* codon 12 mutations were incubated with the indicated concentrations of KR12 for 10 hours at room temperature, followed by the addition of calf thymus DNA. The reaction mixtures were then incubated at 90°C for 5 minutes to cleave DNA strands at their specific alkylated sites. DNA fragments were then recovered by vacuum centrifugation, dissolved in loading dye, denatured at 95°C for 20 minutes, and subjected to electrophoresis on a 6% denaturing polyacrylamide gel.

Cell Culture

Human colon carcinoma-derived HT29 (WT), Caco-2 (WT), SW1463 (12C/12C), SW480 (12V/12V) and SW620 (12V/12V) cells were maintained in Dulbecco’s modified

Eagle's medium (DMEM) supplemented with heat-inactivated 10% FBS, 100 units/mL of penicillin and 100 μg /mL of streptomycin. Human colon carcinoma-derived LS180 (12D/WT) cells were grown in Eagle's minimum essential medium (MEM) containing heat-inactivated 10% FBS, 100 units/mL of penicillin and 100 μg of streptomycin. All cell lines were cultured in a 37°C humidified atmosphere containing 95% air and 5% CO_2.

Cell Proliferation Analysis

Cells were seeded at a final density of 3 x 10^3 or 5 x 10^3 cells/96-well plate and allowed to attach overnight. The cells were then treated with 0.125% DMSO (dimethyl sulfoxide), 50 nM KR12 or #6. Forty-eight hours after treatment, 10 μl of WST-8 reagent (Dojindo) was added to each culture, and the reaction mixtures were incubated at 37°C for another 2 hours. The absorbance readings for each well were performed at 450 nm using a microplate reader (MTP-310; Corona).

Real-time reverse-transcriptase PCR

Total RNA was prepared using the RNAeasy plus mini kit according to the manufacturer's instructions (Qiagen), and 0.5 μg of the RNA was converted to cDNA using the SuperScript VILO cDNA Synthesis System (Invitrogen) according to the manufacturer's protocols. The Q-PCR Master Mix and specific primer sets were used for SYBR Green-based quantitative PCR (Q-PCR) (Applied Biosystems). Three independent measurements were taken, and the amounts were estimated by extrapolation from a standard curve. Expression values were normalised against the expression of *RPS18* and used as an endogenous control. The primer sets used in this study were as follows: *KRAS*, 5'-GGAGAGAGGCCTGCTGAA-3' (sense) and 5'-TGACCTGCTGTGTCGAGAAT-3' (antisense); and *RPS18*, 5'-GAGGATGAGGTGGAACGTGT-3' (sense) and 5'-TCTTCAGTCGCTCCAGGTCT-3' (antisense).

RAS GTP Assay

Cells were washed twice in ice-cold PBS and lysed in Mg^{2+} lysis buffer (MLB; Millipore), and protein concentrations were measured using the Bio-Rad Protein Assay System (Bio-Rad). Equal amounts of cell lysates (500 μg of protein) were mixed with 10 μl of GST-Raf-conjugated agarose beads (Millipore) and incubated for 45 minutes at 4°C. After incubation, the agarose beads were extensively washed in lysis buffer and boiled in 40 μl of

2x SDS-sample buffer for 5 minutes, and the supernatants were analysed by immunoblotting with anti-KRAS antibody (Abcam).

Immunoblot Analysis

Equal amounts of cell lysates prepared from LS180 cells exposed to DMSO, KR12 or #6 were separated by 10% SDS-polyacrylamide gel electrophoresis and electro-transferred onto polyvinylidene difluoride membranes (Immobilon-P; Millipore). The membranes were blocked with TBS-T (Tris-buffered saline plus 0.05% Tween 20) containing 5% non-fat dry milk. After blocking, the membranes were incubated with anti-KRAS (ab55391, Abcam, 1:1000), anti-p21 WAF1 (sc-756, Santa Cruz Biotechnology, 1:1000), anti-p53 (sc-126, Santa Cruz Biotechnology, 1:4000), anti-phospho-p53 at Ser-15 (9284, Cell Signaling Technology, 1:1000), anti-PARP (9542, Cell Signaling Technology, 1:1000), anti-γH2AX (613402, BioLegend, 1:2000), anti-Actin antibody (A5060, Sigma, 1:2000), or anti-BAX (2774, Cell Signaling Technology, 1:1000) followed by incubation with the appropriate HRP (horseradish peroxidase)-conjugated secondary antibody (rabbit:7074, mouse:7076, Cell Signaling Technology). Following extensive washing in TBS-T, antibodies bound to the indicated proteins were visualised using enhanced chemiluminescence reagents (ECL; GE Life Sciences).

Indirect Immunofluorescence Assay

LS180 cells treated with DMSO, KR12 or #6 were rinsed twice in ice-cold PBS and then fixed in 3.7% formaldehyde at room temperature for 30 minutes. After washing in PBS, the cells were permeabilised with 0.1% Triton X-100 in PBS at room temperature for 5 minutes and then blocked with 3% bovine serum albumin (BSA) in PBS at room temperature for 1 hour. After washing in PBS, the cells were incubated with anti-phospho-p53 at Ser-15 or with anti-γH2AX at room temperature for 1 hour, followed by incubation with FITC-conjugated anti-rabbit IgG or rhodamine-conjugated anti-mouse IgG (Invitrogen), respectively, at room temperature for 1 hour. The glass coverslips were washed in PBS and mounted with VectaShield containing DAPI (Vector Laboratories). Fluorescent images were captured using a confocal microscope (Leica).

Flow Cytometry

Cell cycle distribution was examined by flow cytometric analysis with a FACScan flow cytometer (BD Biosciences) following the manufacturer's instructions. In brief, the

attached and floating cells were collected and fixed in ice-cold 70% ethanol. The cells were then stained with a solution containing 50 μg/mL of propidium iodide (PI) and 100 μg/mL of RNase A in PBS at 37°C for 30 minutes to determine the total DNA content. The cell cycle distribution was then analysed using a FACScan flow cytometer.

Animal Tumour Models

The animal protocol was approved by Chiba Cancer Center Animal Ethics Committee. HT29 (WT), LS180 (12D/WT) or SW480 (12V/12V) cells were implanted s.c. into the dorsal flanks of 6-week-old female athymic mice (Supplementary Fig. 6 (a)). When the tumour volume reached 100 mm^3, administration of a non-toxic dose of DMSO or KR12 (320 μg/kg body weight) was performed, and 5 subsequent weekly injections with DMSO or KR12 were administered through their tail veins. Tumour-bearing mice were euthanised at the indicated times over 12 weeks after the first administration or when the tumours exceeded 2 cm in diameter.

Statistical Evaluation

Statistical analyses of the experimental data were performed using Student's *t*-test. The statistical significance of tumour growth between the treated and control groups was assessed using the statmod software package for R (http://wwww.r-project.org) [1]. The initial set at a p value of <0.05.

Acknowledgements

The authors are grateful to Y. Hirano and Y. Suzuki for technical assistance. This work was supported by a Grant-in-Aid for Scientific Research (B) # 23300344 and in Innovative Areas # 25134718 and by a Project for the Development of Innovative Research on Cancer Therapeutics (P-Direct) and Young Scientists (B) #13307606 from the Ministry of Education, Culture, Sports, Science and Technology, Japan.

Author Contributions

H.N. planned and oversaw the project. T.W., R.D.T., T.B., H.S. and H.N. designed the chemicals, and T.W., R.D.T., and T.B synthesised the chemicals. The bulk of the *in vitro* experiments were performed by K.H. and the bulk of the *in vivo* experiments were performed by T.I., all under the supervision of T.O. and H.N., with technical support from H.Y., H.S., K.F., N.K. and Y.M. K.H. and H.N. performed the statistical analyses. K.H., T.I., T.W., K.S., T.O., T.B., H.S., T.D. and H.N. discussed and interpreted all data. K.H., T.O. and H.N. wrote the manuscript, with input from the other authors. A.B. contributed critical comments to the experimental strategy and editing. A.T., together with K.H., performed the experiments described in Supplementary Fig. 3 and Supplementary Fig. 5.

FIGURE LEGENDS

Figure 1. Structure of KR12 and the sequence-specific cleavage of a DNA strand through KR12-dependent alkylation. **(a)**, chemical structure of the PI polyamide *seco*-CBI conjugate, termed KR12. **(b)**, schematic drawing of thermal-induced cleavage at the sites of *KRAS* codon 12 mutations. The upper and lower panels represent the G12V;GTT and G12D;GAT mutations. Circles represent imidazole moieties, and arrows indicate the positions of KR12-dependent alkylation and cleavage. An increased level of specific cleavage products was seen with increasing doses of KR12 (from bottom to top, Fig. 1 (b))

Figure 2. KR12-mediated specific suppression of KRAS codon 12 mutants in human colon cancer cells. **(a),** WST assay. Human colon cancer cells expressing wild-type KRAS, including HT29 and Caco-2, or human colon cancer cells harbouring *KRAS* codon 12 mutations, including SW1643, SW480, SW620 and LS180, were incubated with the indicated concentrations of KR12. Forty-eight hours after treatment, the per cent viable cells were examined by WST assay and depicted in a line graph. Error bars indicate the SDs of the data from triplicate experiments. **(b)**, quantitative rtPCR analysis. Relative KRAS expression 48 hours after treatment with DMSO, KR12, #6 or Dp was plotted as a bar graph. Error bars indicate the SDs of data from triplicate experiments. **(c)**, allele-specific downregulation of *KRAS* codon 12 mutant: cDNA from the treated RNA was subcloned. Transfected antibiotic-resistant/colour-selected colonies were screened by colony PCR and direct colony sequencing methods. The number of colonies for the wild-type or codon 12 *KRAS* mutant allele of each treated group was counted and reported in the table. The percentages of wild-type and mutant *KRAS* sequences are also shown in parentheses. **(d)**, immunoblot analysis. Immunoblots for anti-KRAS or anti-actin antibody (top and bottom panels, respectively) for LS180 (12D/WT) and HT29 (WT) cells 48 hours after the treatment with either control DMSO solution, KR12 or #6. The GST-Raf-bound proteins from each treated group were pulled-down and analysed by immunoblotting with anti-RAS antibody (middle panels).

Figure 3. KR12-dependent induction of cellular senescence and apoptosis. **(a)**, SA-β-gal staining. LS180 cells were exposed to DMSO, KR12 or #6 (at a final concentration of 50 nM). Forty-eight hours after treatment, phase-contrast microphotographs were taken (top panels), and the cells were washed in PBS, fixed in 2% formaldehyde plus 0.05% glutaraldehyde and incubated with SA-β-gal staining solution containing X-gal for 24 hours at 37°C (bottom

panels). **(b)**, cell cycle distribution analysis. Forty-eight hours (top) and two weeks (bottom) after treatment, cells were subjected to FACS analysis, and the DNA contents of each sample were analysed and depicted following the manufacturer`s instructions. **(c)**, DNA fragmentation. The attached and floating LS180 cells 48 hours (left) and two weeks (right) after treatment were collected, and their genomic DNA was prepared and analysed by 1% agarose gel electrophoresis with λ/*Hin*dIII and ϕ-X174/*Hae*III size markers. **(d)**, immunoblotting. Forty-eight hours (left) and two weeks (right) after the treatment, whole cell lysates were prepared and subjected to immunoblotting with the indicated antibodies. Actin was used as a loading control.

Figure 4. KR12 suppresses tumour growth *in vivo*. **(a)**, The indicated human colon cancer cells, i.e., HT29 (WT), LS180 (12D/WT) and SW480 (12V/12V), were injected s.c. into BALB/c nude mice. When the tumour volume reached 100 mm^3, DMSO or KR12 (320 μg/kg body weight) was i.v. injected through the tail vein every 7 days. At the indicated times after administration, the tumour volume was calculated as the longest diameter x $width^2$ x 0.5. The mean tumour volume, with SEs (open circles for DMSO and closed circles for KR12 treatment), and mean body weight, with SEs (open triangles for DMSO and closed triangles for KR12 treatment), of the KR12-treated group and control group are plotted in a line graph with error bars (SEs). The numbers of animals used were 6 for HT29 (DMSO and KR12) and LS180 (KR12), 5 for LS180 (DMSO) and SW480 (KR12), and 8 for SW480 (DMSO). **(b),** images of the euthanised mice of each group are shown. An image of an SW480 xenograft 5 weeks after KR12 treatment, which was the final treatment, is also shown.

References

[1] T. Baldwin, et al., "Wound healing response is a major contributor to the severity of cutaneous leishmaniasis in the ear model of infection," Parasite Immuno 29(10), 501 (2007).
[2] T. Bando, et al., "Efficient DNA alkylation by a pyrrole-imidazole CBI conjugate with an indole linker: sequence-specific alkylation with nine-base-pair recognition," Bioconjugate Chemistry 17(3), 715 (2006).
[3] T. Bando and H. Sugiyama, "Synthesis and biological properties of sequence-specific DNA-alkylating pyrrole-imidazole polyamides," Accounts of Chemical Research 39(12), 935 (2006).
[4] J. Campisi, "Aging, cellular senescence, and cancer," Annual Review of Physiology 75, 685 (2013).
[5] M. Collado and M. Serrano, "Senescence in tumours: evidence from mice and humans," Nat.Rev.Cancer 10(1), 51 (2010).
[6] P. B. Dervan, "Molecular recognition of DNA by small molecules," Bioorganic & Medicinal Chemistry 9(9), 2215 (2001).
[7] L.A. Dickinson et al. "Arresting cancer proliferation by small-molecule gene regulation," Chem Biol. 11, 1583-1594 (2004).
[8] C. Jespersen et al. "Chromatin structure determines accessibility of a hairpin polyamide-chlorambucil conjugate at histone H4 genes in pancreatic cancer cells," Bioorg Med Chem Lett. 12, 4068-4071 (2012).
[9] C. Lengauer et al. "Cancer drug discovery through collaboration." Nature Reviews Drug Discovery 4, 375-380 (2005)
[10] Y. Liu and W. F. Bodmer, "Analysis of P53 mutations and their expression in 56 colorectal cancer cell lines," Proc.Natl.Acad.Sci.U.S.A. 103(4), 976 (2006).
[11] H. Matsuda, et al., "Transcriptional inhibition of progressive renal disease by gene silencing pyrrole-imidazole polyamide targeting of the transforming growth factor-beta1 promoter," Kidney Int. 79(1), 46 (2011).
[12] J. Neumann, et al., "Frequency and type of KRAS mutations in routine diagnostic analysis of metastatic colorectal cancer," Pathol. Res. Pract. 205(12), 858 (2009).
[13] J. M. Ostrem, et al., "K-Ras(G12C) inhibitors allosterically control GTP affinity and effector interactions," Nature 503(7477), 548 (2013).
[14] R. Perez, et al., "A view on EGFR-targeted therapies from the oncogene-addiction perspective," Front. Pharmacol. 4, 53 (2013).
[15] J.A. Raskatov et al. “Tumor xenograft uptake of a pyrrole-imidazole (py-im) polyamide varies as a function of cell line grafted.” J Med Chem 57(20):8471-6 (2014).
[16] M. Rokita, et al., "Overexpression of epidermal growth factor receptor as a prognostic factor in colorectal cancer on the basis of the Allred scoring system," OncoTargets Ther. 6, 967 (2013).
[17] F. Shima, et al., "In silico discovery of small-molecule Ras inhibitors that display antitumor activity by blocking the Ras-effector interaction," Proc.Natl.Acad.Sci.U.S.A. 110(20), 8182 (2013).
[18] R. D. Taylor, et al., "Sequence-Specific DNA Alkylation Targeting for Kras Codon 13 Mutation by Pyrrole-Imidazole Polyamide seco-CBI Conjugates," Eur. J Chemistry 20(5):1310 (2014).
[19] The American Cancer Society, "American Cancer Society. Cancer Facts & Figures 2013. Atlanta: American Cancer Society; 2013.,"(2013).

[20] L. Tortolina, et al., "A multi-scale approach to colorectal cancer: from a biochemical-interaction signaling-network level, to multi-cellular dynamics of malignant transformation. Interplay with mutations and onco-protein inhibitor drugs," Curr. Cancer Drug Targets 12(4), 339 (2012).
[21] X. Wang, et al., "Inhibition of MMP-9 transcription and suppression of tumor metastasis by pyrrole-imidazole polyamide," Cancer Science 101(3), 759 (2010).
[22] Y.D.Wang et al, "Cell-free and cellular activities of a DNA sequence selective hairpin polyamide-CBI conjugate." J. Biol. Chem., 277, 42431–42437 (2002).
[23] N.R Wurtz and P.B Dervan. "Sequence specific alkylation of DNA by hairpin pyrrole-imidazole polyamide conjugates." Chem. Biol., 7, 153–161(2000)
[24] F. Yang, et al., "Antitumor activity of a pyrrole-imidazole polyamide," Proc.Natl.Acad.Sci.U.S.A. 110(5), 1863 (2013).
[25] G. Zimmermann, et al., "Small molecule inhibition of the KRAS-PDEdelta interaction impairs oncogenic KRAS signalling," Nature 497, 631 (2013).

Hiraoka *et al.*, Figure 1

a

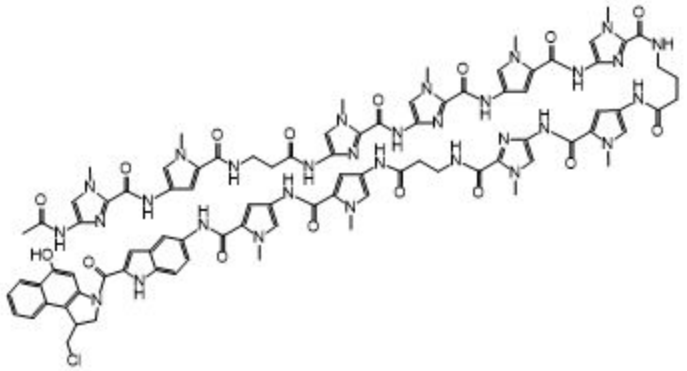

b

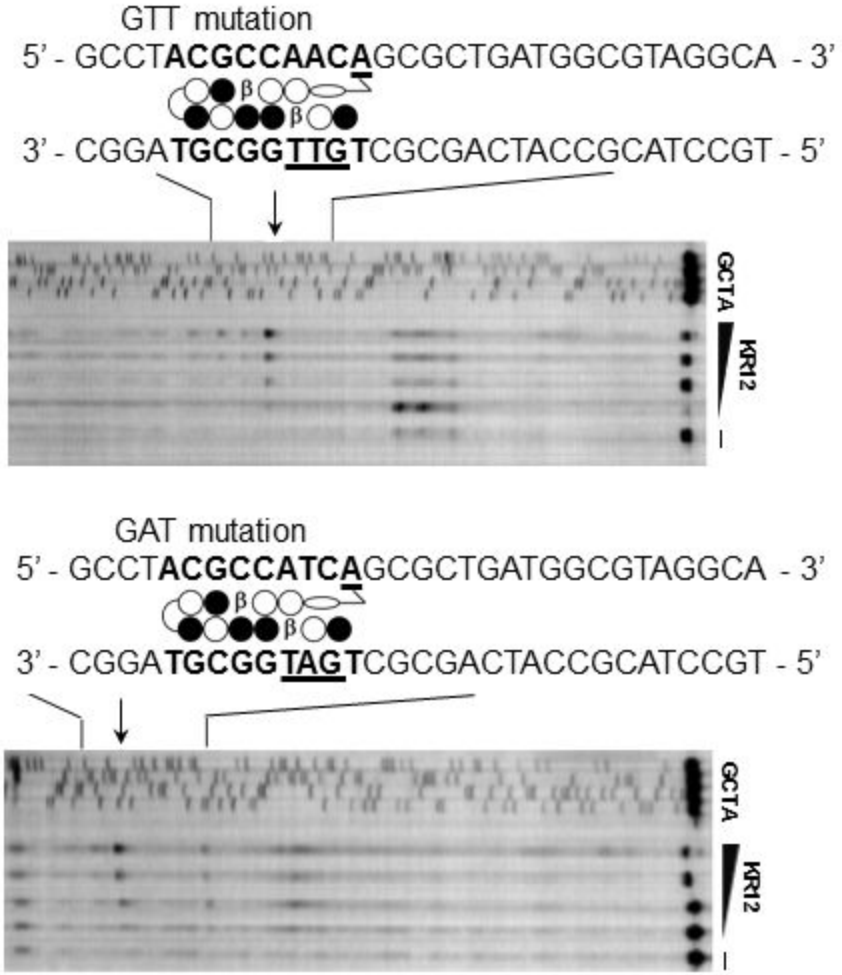

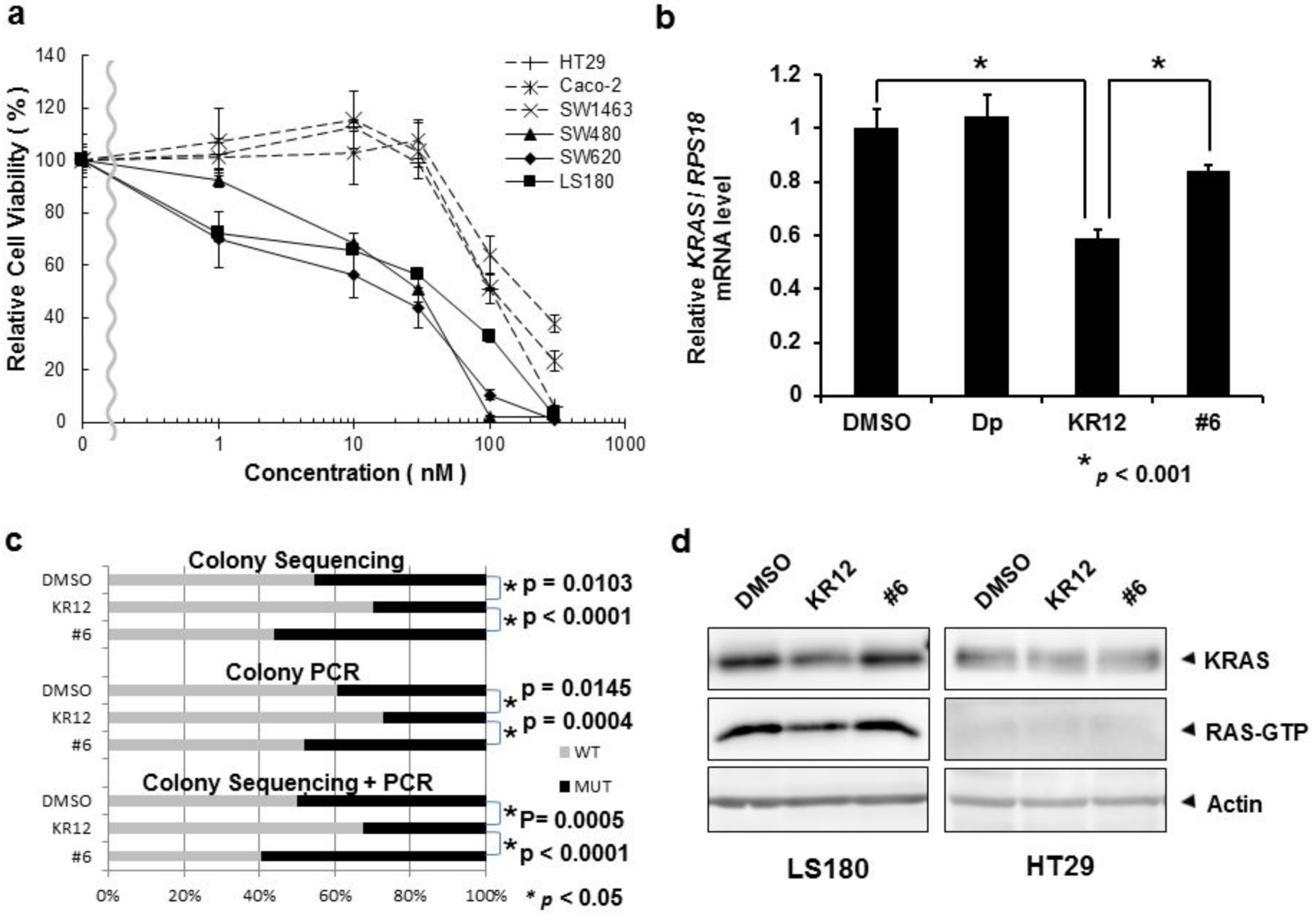
a
Relative Cell Viability (%)
Concentration (nM)
HT29
Caco-2
SW1463
SW480
SW620
LS180
b
Relative KRAS / RPS18 mRNA level
DMSO
Dp
KR12
#6
* p < 0.001
c
Colony Sequencing
* p = 0.0103
* p < 0.0001
Colony PCR
p = 0.0145
p = 0.0004
WT
MUT
Colony Sequencing + PCR
P= 0.0005
p < 0.0001
* p < 0.05
d
DMSO
KR12
#6
KRAS
RAS-GTP
Actin
LS180
HT29

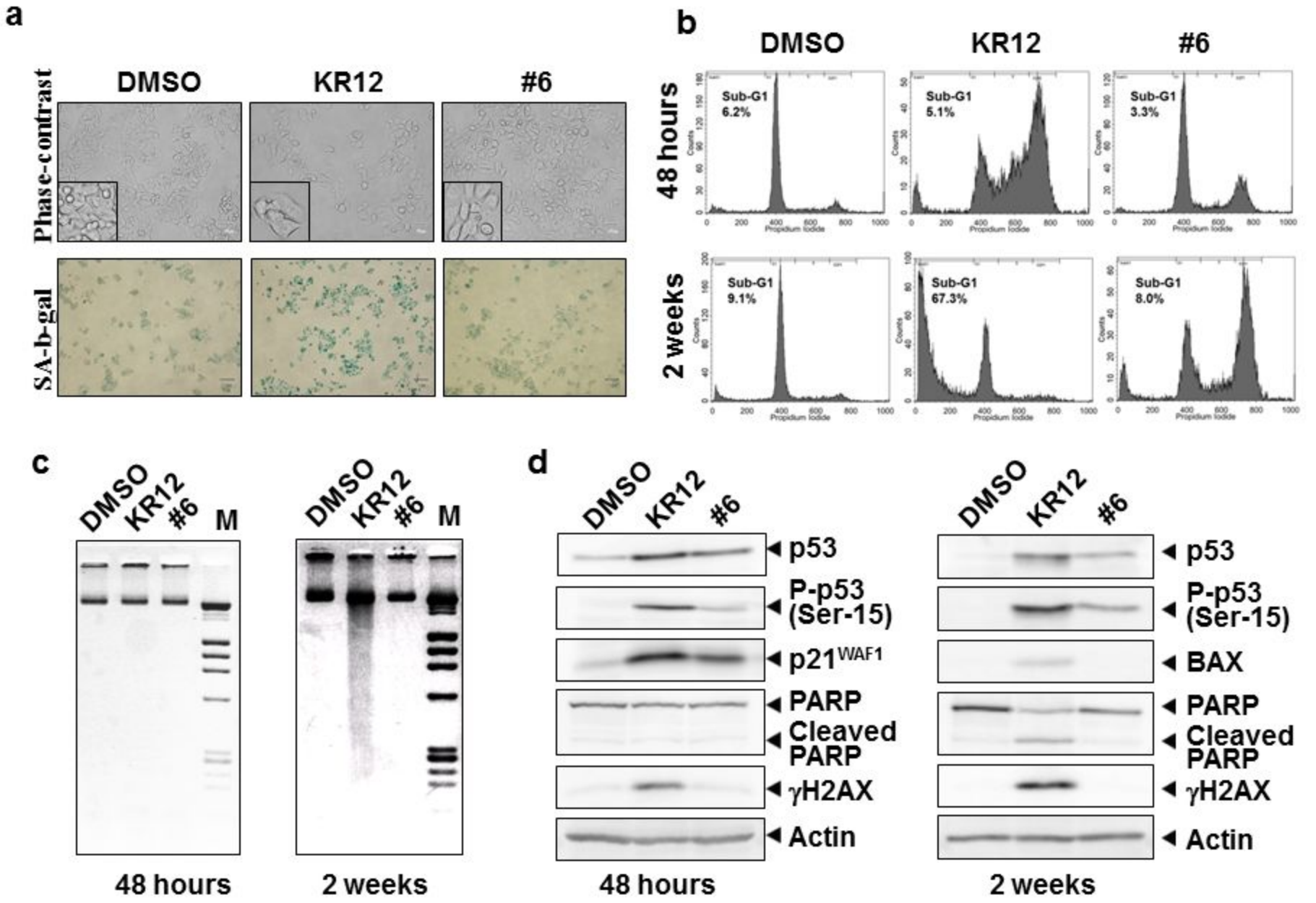
a
DMSO
KR12
#6
Phase-contrast
SA-b-gal
b
DMSO
KR12
#6
48 hours
2 weeks
Sub-G1
6.2%
Sub-G1
5.1%
Sub-G1
3.3%
Sub-G1
9.1%
Sub-G1
67.3%
Sub-G1
8.0%
Counts
Propidium Iodide
c
DMSO
KR12
#6
M
48 hours
2 weeks
d
DMSO
KR12
#6
p53
P-p53
(Ser-15)
p21WAF1
PARP
Cleaved
PARP
γH2AX
Actin
BAX
48 hours
2 weeks

a

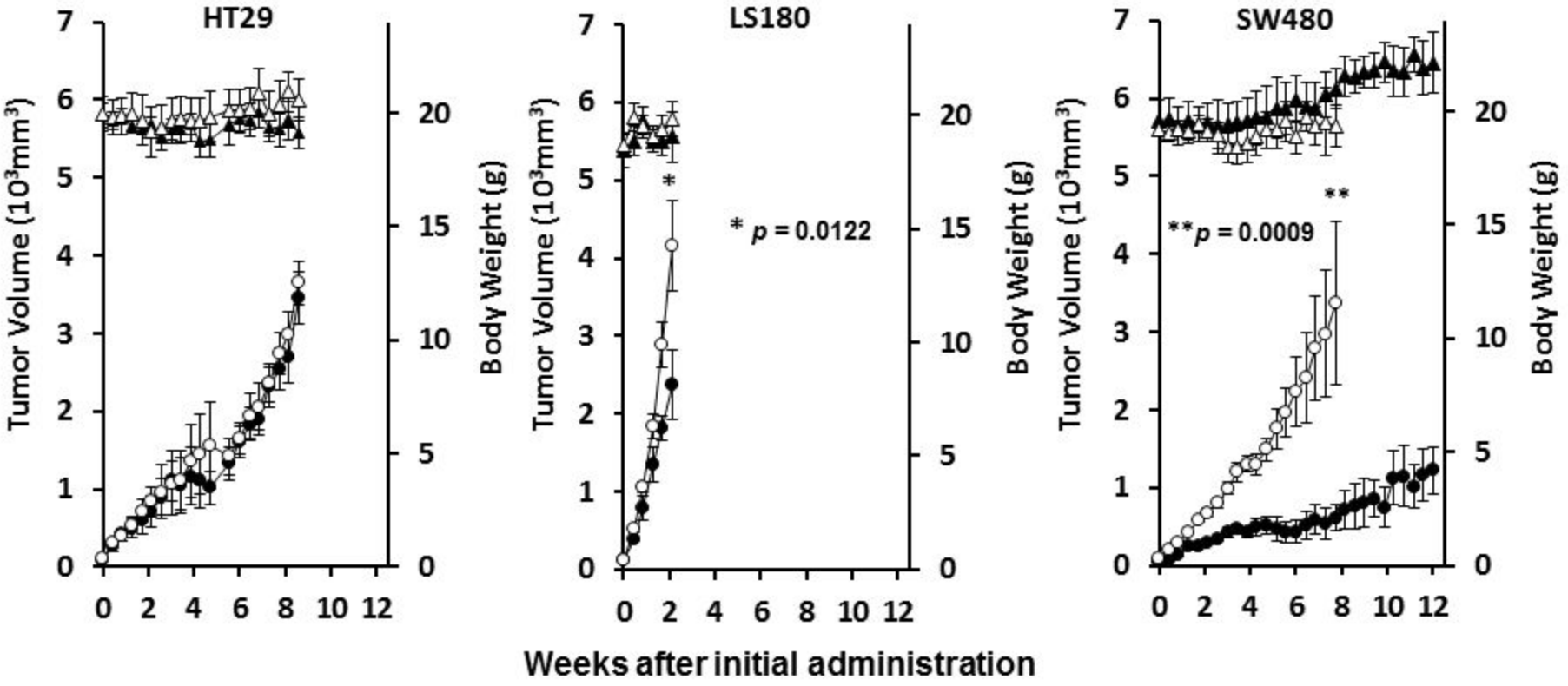
HT29
LS180
SW480
Tumor Volume (10³mm³)
Body Weight (g)
* p = 0.0122
** p = 0.0009
Weeks after initial administration

b

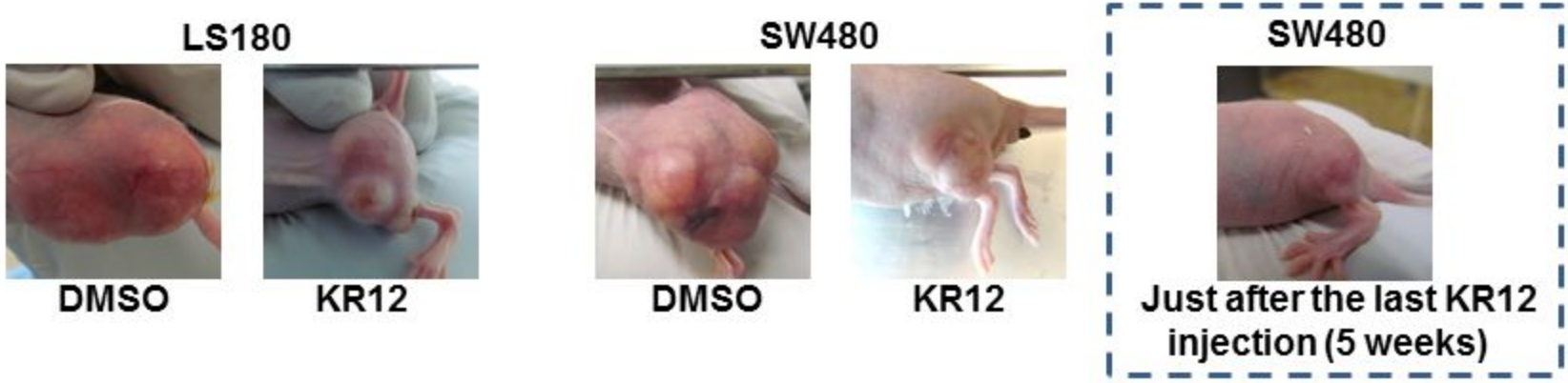
LS180
SW480
SW480
DMSO
KR12
DMSO
KR12
Just after the last KR12 injection (5 weeks)

Supplementary Figures and Tables

Hiraoka *et al.*

Inhibition of KRAS codon 12 mutants using a novel DNA-alkylating pyrrole-imidazole polyamide conjugate

Supplementary Figure 1

a

b

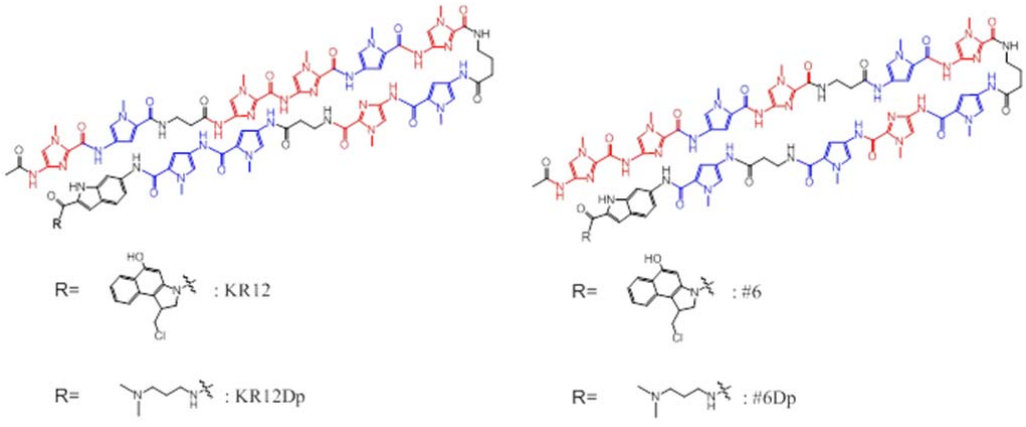

c

KR12Dp/ wt

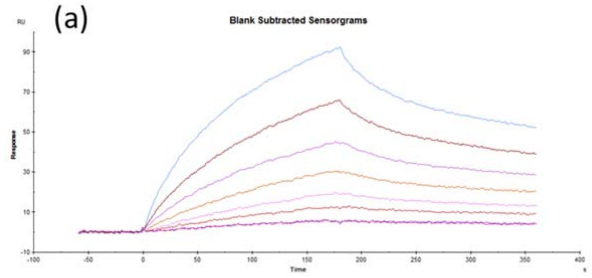

KD= 1.14×10^{-7}

KR12Dp/ GAT

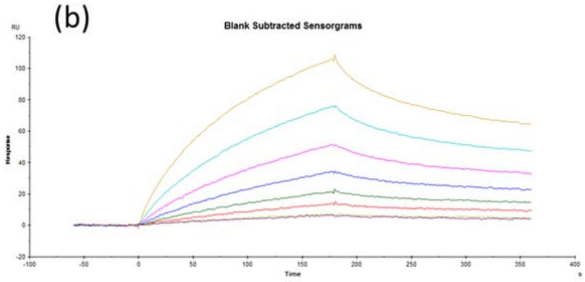

KD= 8.47×10^{-9}

KR12Dp/ GTT

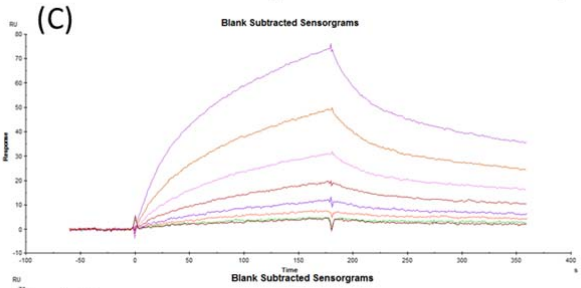

KD= 1.71×10^{-8}

#6 Dp/ wt

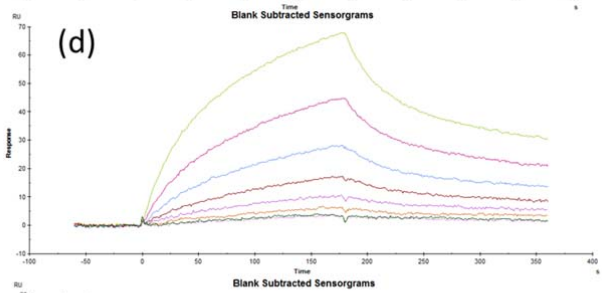

KD= 2.62×10^{-7}

#6 Dp/ GAT

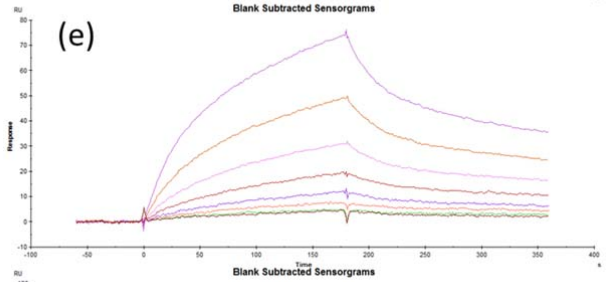

KD= 2.27×10^{-7}

#6 Dp/ GTT

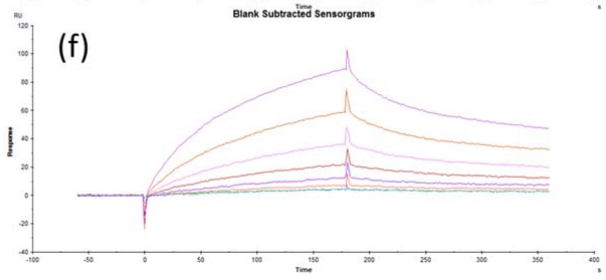

KD= 2.47×10^{-7}

DNA binding between biotinylated hairpin DNAs and Pyrrole-Imidazole polyamides, KR12Dp and #6Dp. **a.** Biotin-labelled hairpin oligos were designed and synthesised to generate double-strand DNA, including wild-type (GGT 12G) and two mutant (GAT 12D and GTT 12V) sequences. The WT (GGT) DNA was the 1 base mismatch sequence for KR12. The MUT (GAT) and MUT (GTT) sequences were full-match sequences for KR12. **b.** KR12 and #6 have alkylating seco-CBI moieties. KR12Dp and #6Dp have DP to be used for the SPR assay. **c.** SPR assays for KR12Dp and #6Dp with either WT (GGT), MUT (GAT) or MUT (GTT) DNAs at concentrations of 12.5 nM, 25 nM, 50 nM, 100 nM, 200 nM, 400 nM, or 800 nM in HBS-EP buffer with 0.1% DMSO were performed. Sensorgrams of KR12Dp and #6Dp with each biotinylated hairpin oligo, i.e., (a) KR12Dp with WT (GGT), (b) KR12Dp with MUT (GAT), (c) KR12Dp with MUT (GTT), (d) #6Dp with WT (GGT), (e) #6Dp with MUT (GAT) and (f) #6Dp with MUT (GTT), are shown.

Supplementary Figure 2

a

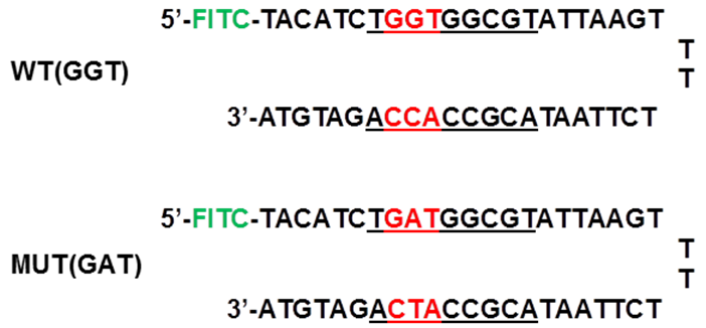

b

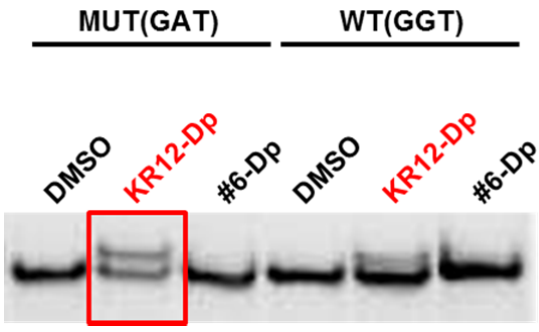

Gel shift assays for sequence-specific binding of KR12-Dp targeting KRAS codon 12 mutation sequences **a.** Two FITC-labelled hairpin oligos for the wild-type and mutant were designed and synthesised to generate double-strand DNA, including WT (GGT) and MUT (GAT) sequences. Double-strand DNAs were generated by heat denaturation at 100°C for 5 minutes in annealing buffer (10 mM Tris, pH 7.5–8.0, 50 mM NaCl, 1 mM EDTA) and subsequent slow cooling to room temperature for more than 120 minutes. **b.** The gel shift assay was performed as previously described [17]. Briefly, 7.5 pmol of FITC-labelled oligonucleotides were incubated with 75 pmol of KR12Dp or #6Dp for 1 hour at 37°C. The resulting complexes were separated by electrophoresis and visualised with the luminescent image analyser LAS-4000 (Fujifilm, Tokyo, Japan). KR12Dp and WT DNA complexes showed remarkable gel shifts, while the other complexes did not.

Supplementary Figure 3

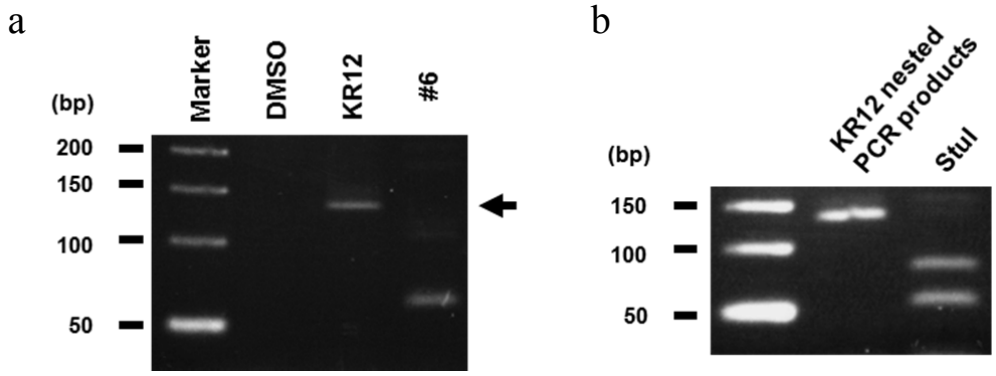

Endogenous alkylation confirmed by Ligation-mediated PCR LS180 cells were plated at a density of 5 × 10^5 cells/10-cm dish and exposed to 500 nM of KR12 or #6. Twenty-four hours after treatment, genomic DNA was extracted by phenol-chloroform extraction and ethanol precipitation, and the alkylated genomic DNA (1 μg) was heated at 98°C for 2 minutes. First-strand synthesis was performed using Prime STAR HS DNA polymerase (TAKARA) with a first-strand primer (5'- TACGATACACGTCTGCAGTCAAC-3'). After phenol extraction and ethanol precipitation, the sample DNA was resuspended in 25 μL of water, and the resuspended DNA (4 μL) was subjected to ligation with pre-annealed linker DNAs (Linker 1: 5'-AGCACTCTCGAGCCTCTCACCGCA-3' and Linker 2: 5'-TGCGGTGAGAGG-3') at 16°C overnight using a DNA ligation kit (DNA Ligation Kit, Ver 2.1, TAKARA). To detect the DNA fragment ligated with the linker, we performed PCR using a primer pair (5'-CACGTCTGCAGTCAACTGGAAT-3' and 5'-AGCACTCTCGAGCCTCTCA-3') followed by nested PCR using a primer pair (5'-TTATGTGTGACATGTTCTAATATAGTCAC-3' and 5'-CTCTCGAGCCTCTCACC-3'). **a.** PCR fragments were electrophoresed in a 4% agarose gel, and the expected PCR fragments were detected using an UV illuminator: #6 showed a short fragment of DNA, suggesting that the non-dose-dependent thermal cleavage site approximately 60 bp upstream of the mutation site was detected by this method. **b.** The amplified DNA fragment should have *Stu*I restriction enzyme sites and should generate 57 new fragments after digestion by *Stu*I. The fragments were confirmed by restriction enzyme digestion with *Stu*I.

Supplementary Figure 4

a

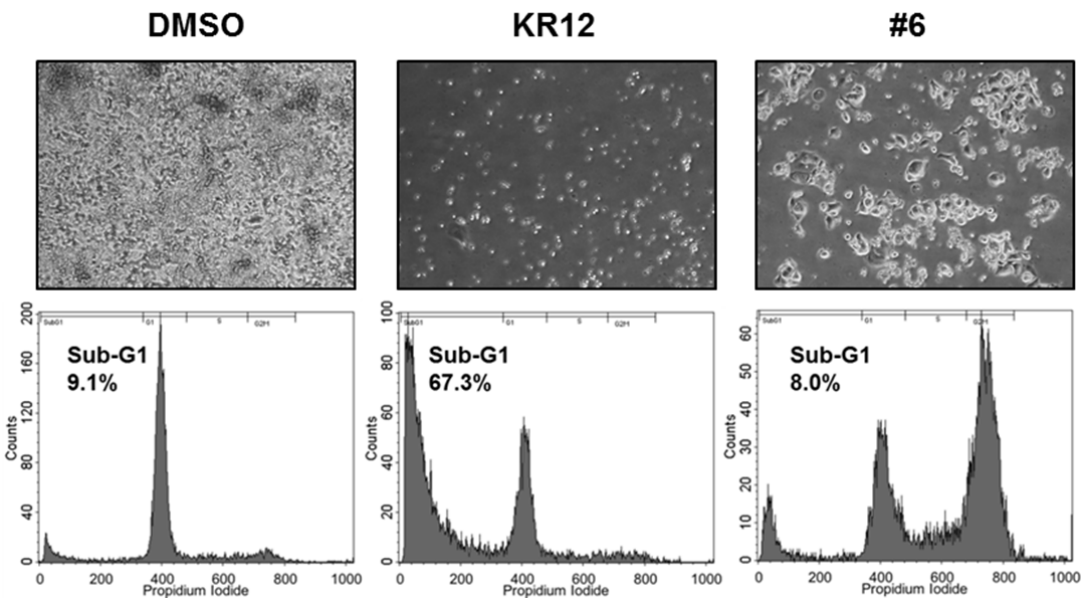

b

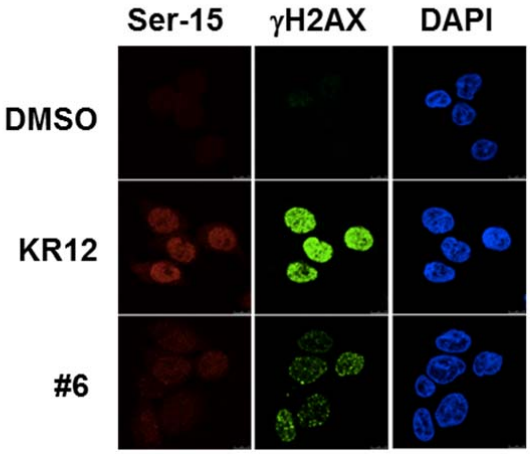

c

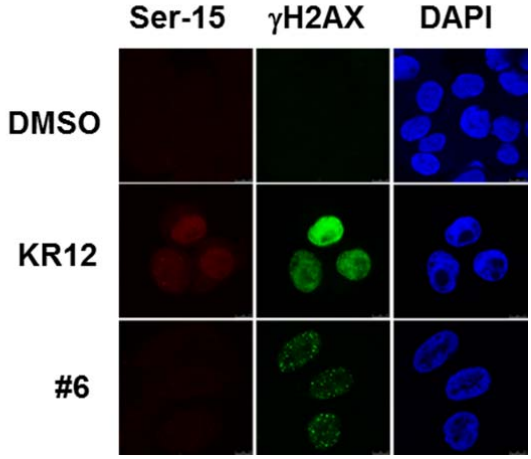

d

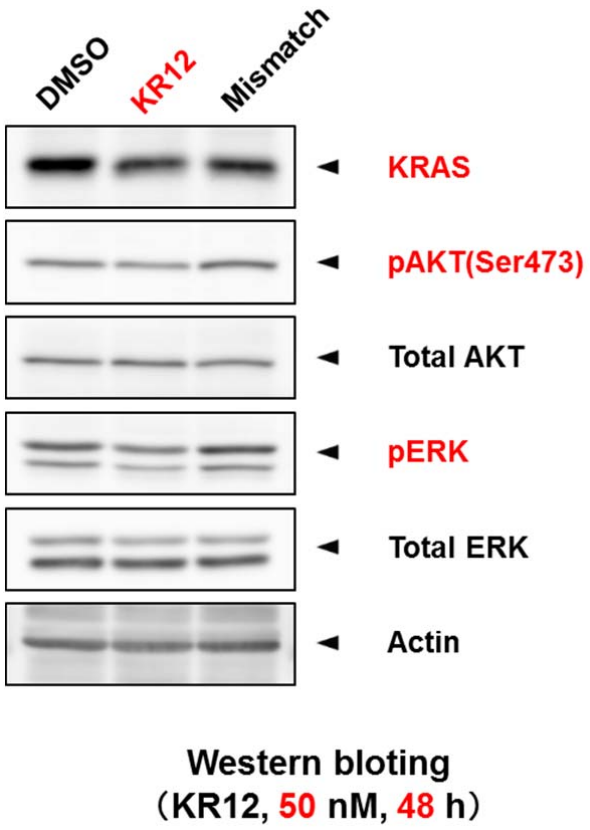

Cell cycle distribution after long-term treatment, DNA damage induction and KRAS downstream. **a.** Two weeks after treatment with the control 0.125% DMSO solution, 50 nM KR12 or #6, phase-contrast microphotographs of LS180 cells were taken and are shown (top panels). The adherent and floating cells were then collected and subjected to FACS analysis to determine the cell cycle distribution (bottom panels). **b.** LS180 cells were subjected to the same DMSO, KR12 or #6 treatments. Forty-eight hours after treatment, the cells were fixed and simultaneously incubated with polyclonal anti-Phospho-p53 at Ser-15 (red) and monoclonal anti-γH2AX (green) antibodies. Cell nuclei were stained with DAPI (blue). Images were taken by confocal microscopy. **c.** Two-week KR12 exposure-mediated accumulation of phospho-p53 at Ser-15 and γH2AX, detected by indirect immunofluorescence assays. LS180 cells were treated with DMSO, KR12 or #6 for two weeks and then fixed and simultaneously incubated with polyclonal anti-Phospho-p53 at Ser-15 (red) and monoclonal anti-γH2AX (green) antibodies. Cell nuclei were stained with DAPI (blue). Images were taken by confocal microscopy. **d.** LS180 cells were treated with 50 nM KR12 for 48 hours. Extracted proteins from the treated cells were subjected to SDS-PAGE and subsequent Western blotting. KR12 induced a slight reduction in KRAS, phospho-AKT and phospho-ERK expression.

Supplementary Figure 5

a

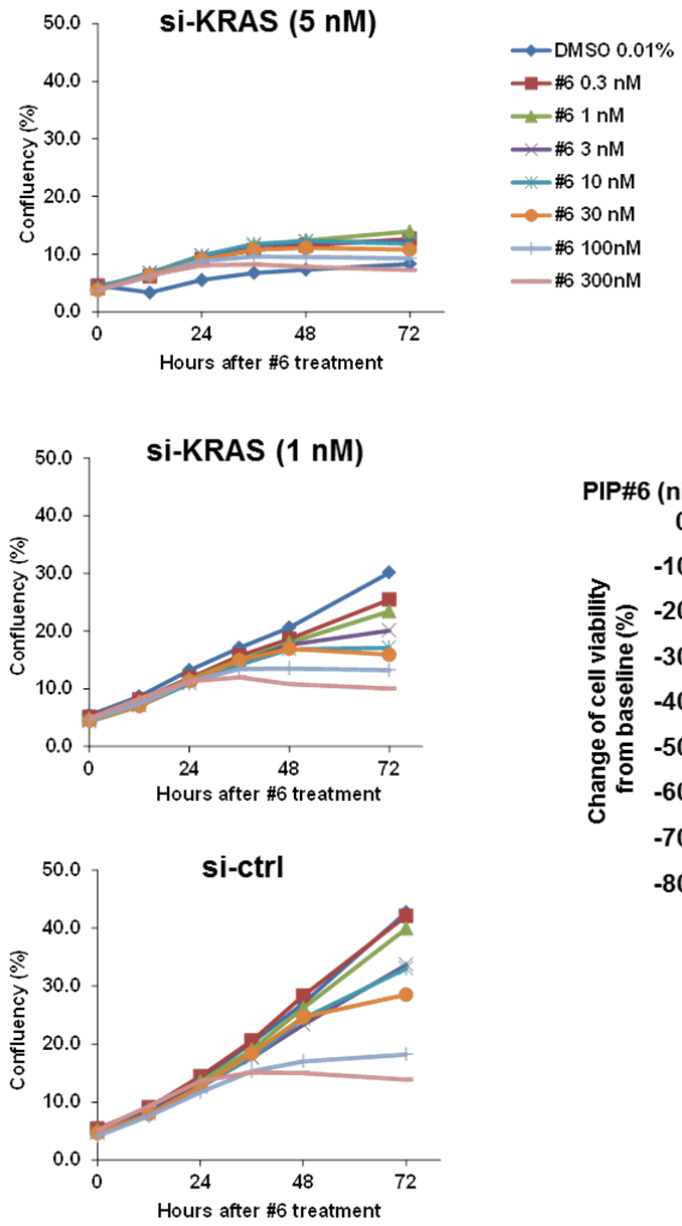

b

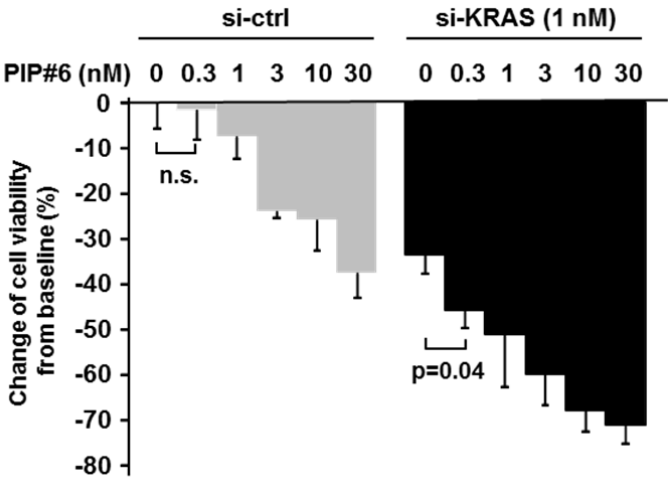

KRAS suppression enhance DNA alkylator induced cell growth arrest. To knockdown the expression of KRAS genes, LS180 cells were transfected with 5 nM of the indicated siRNAs against mutated KRAS (Réjiba, et al., Cancer Sci 98(7): 1128–1136 2007) using Lipofectamine-RNAiMAX (Invitrogen) according to the manufacturer's recommendations. Seventy-two hours after transfection, cell proliferation was assessed using a real-time cell

imaging system (IncuCyte; Essens Bioscience). For co-treatment with #6, LS180 cells were transfected with siRNA against mutated KRAS (1 or 5 nM), and 24 hours after transfection, the cells were treated with the indicated concentration of #6 for 72 hours.

a. The LS180 cells treated with 5 nM of KRAS siRNA showed nearly complete suppression of KRAS expression and cell growth in LS180 cells (top), while 1 nM of KRAS siRNA showed partial suppression of KRAS expression (50%) and cell growth (middle). The control siRNA (si-ctrl) did not suppress KRAS expression or cell growth (bottom). Non- and partial-KRAS suppression due to #6 treatment resulted in dose-dependent suppression of cell growth. **b.** The Waterfall plot shows reduced viability of LS180 cells, and accordingly, significant growth inhibition (P=0.04) was observed after the administration of even low concentrations (0.3 nM) of #6 after pre-exposure with 1 nM of the KRAS siRNA for 24 hours. Error bars indicate the SDs of the data from triplicate experiments.

Supplementary Figure 6

a

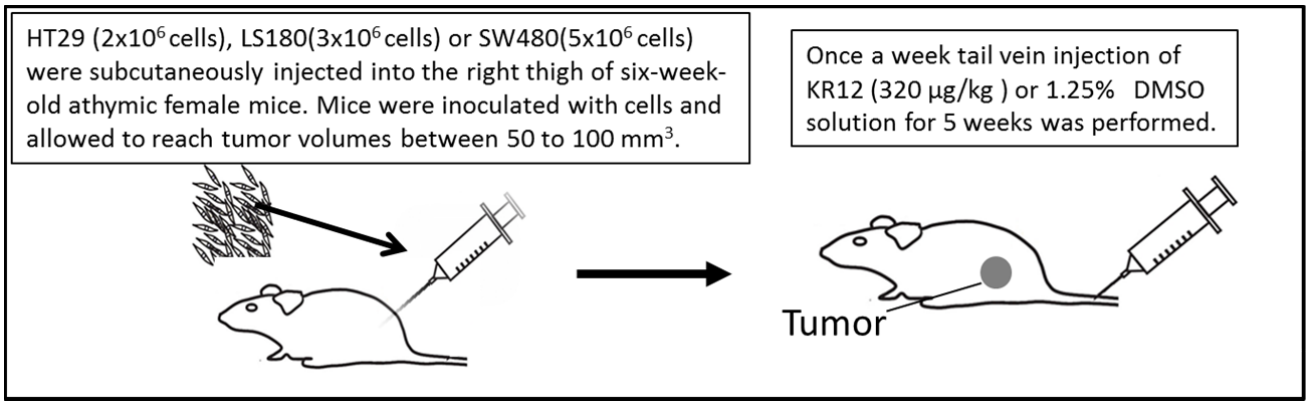

b

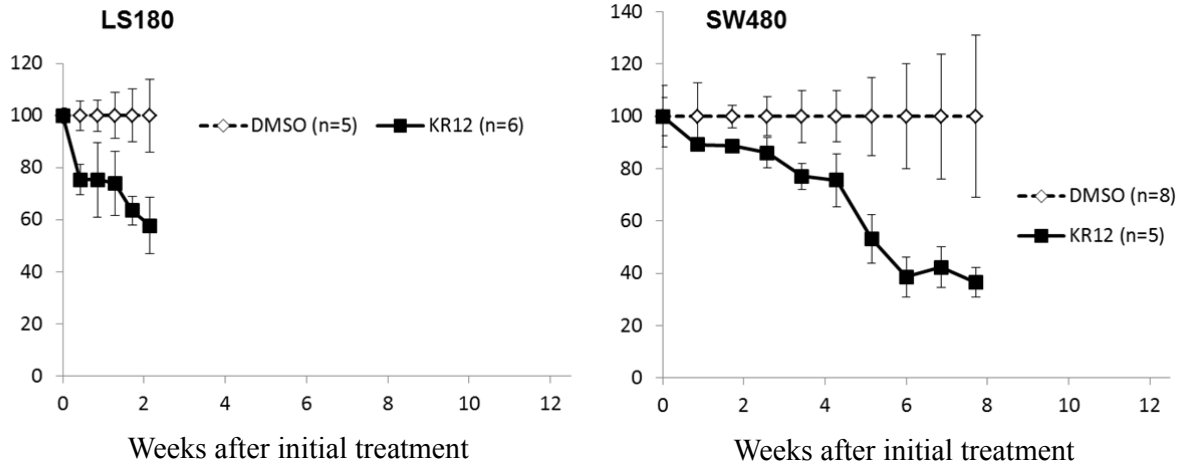

Establishment of human colorectal cancer xenograft models and relative tumour growth inhibition by KR12. **a.** A schematic figure of tumour cell implantation and inoculation and subsequent administration of KR12 is shown. The animals were euthanised when the tumours reached a maximum of 10% body weight or when an individual tumour or the sum of all tumours reached a size of 2.0 cm in diameter. The animals were also euthanised before this stage if they showed signs of distress, loss of body weight (20%) or departure from the normal behaviour during the study, as under the IACUC protocol. **b.** The average relative tumour sizes, with error bars, were blotted every three days after the initial treatment for the

LS180 xenograft model (left) and once a week for the SW480 (right) xenograft model. Open diamond dotted lines indicate the DMSO-treated group, and black square lines indicate the KR12-treated group. Error bars indicate the SEs of the data from the indicated number of animal experiments.

Supplementary Figure 7

a

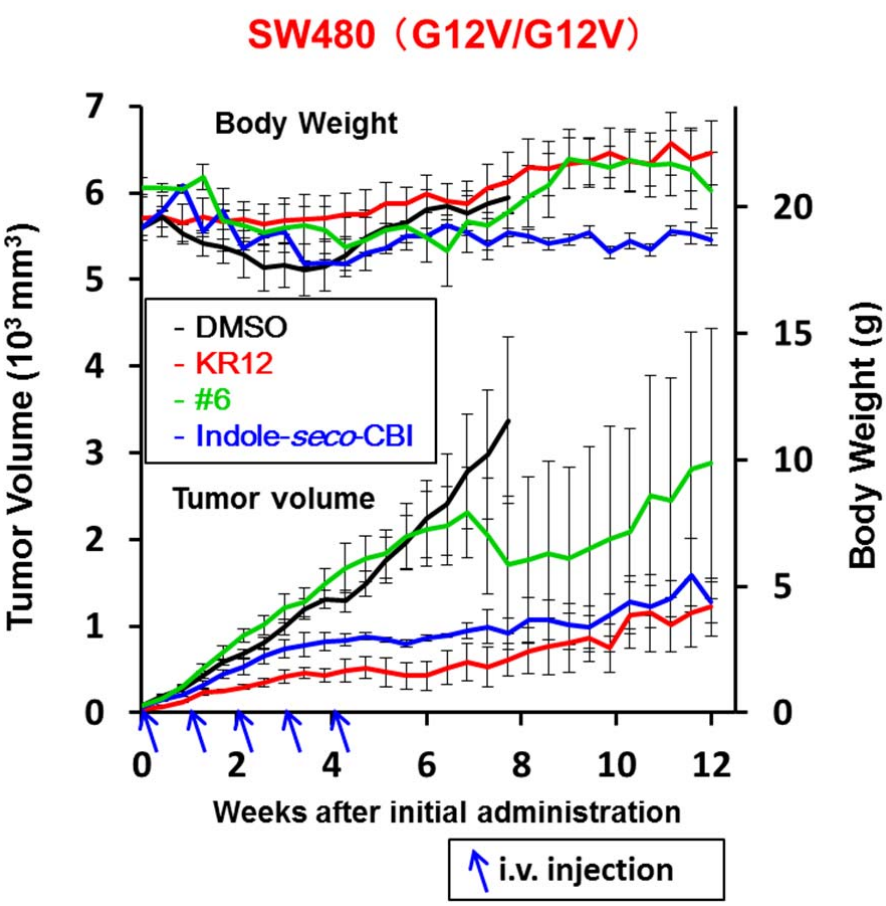

b

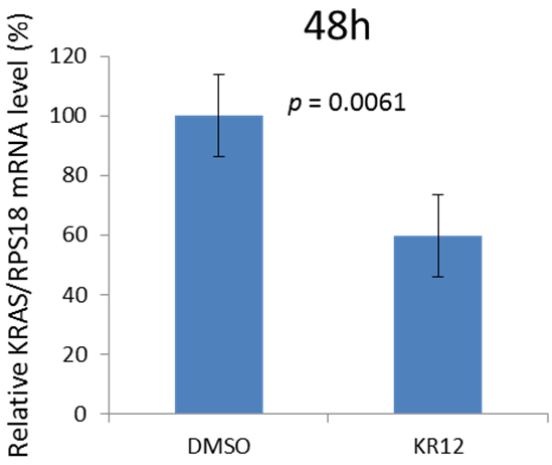

Tumour growth inhibition of SW480 xenograft model and inhibition of KRAS expression in xenografted tumours. Animal experiments were performed as described in

Figure 4 and Supplementary Figure 6. **a.** In this study, we added experiments using #6 (4 animals) and indole-seco-CBI (4 animals) treatment to the human colorectal cancer SW480 xenograft model as well as the KR12 (5 animals) and DMSO (8 animals) treatments. KR12, but not indole-seco-CBI, showed a significant reduction in tumour size over that of #6 (P=0.0061). Indole-seco-CBI-treated animals showed no body weight gain and slight illness compared to mice treated with the DMSO control and to mice treated with PI polyamide indole-seco-CBIs (KR12 and #6). Vertical error bars indicate ± SEs. **b.** Each of four LS180 xenografted tumours, 48 hours after DMSO or KR12 treatment (4 animals each), was collected and subjected to RNA preparation followed by real time quantitative PCR experiments to assess KRAS gene expression using the same primer sets used in Figure 2. All four KR12-treated tumours showed lower KRAS expression levels than all four DMSO-treated tumours. Significant suppression of KRAS expression by KR12 is shown in a bar graph of the mean values of 4 expression analyses, with vertical bars representing the standard deviation (P=0.0061).

Supplementary Figure 8

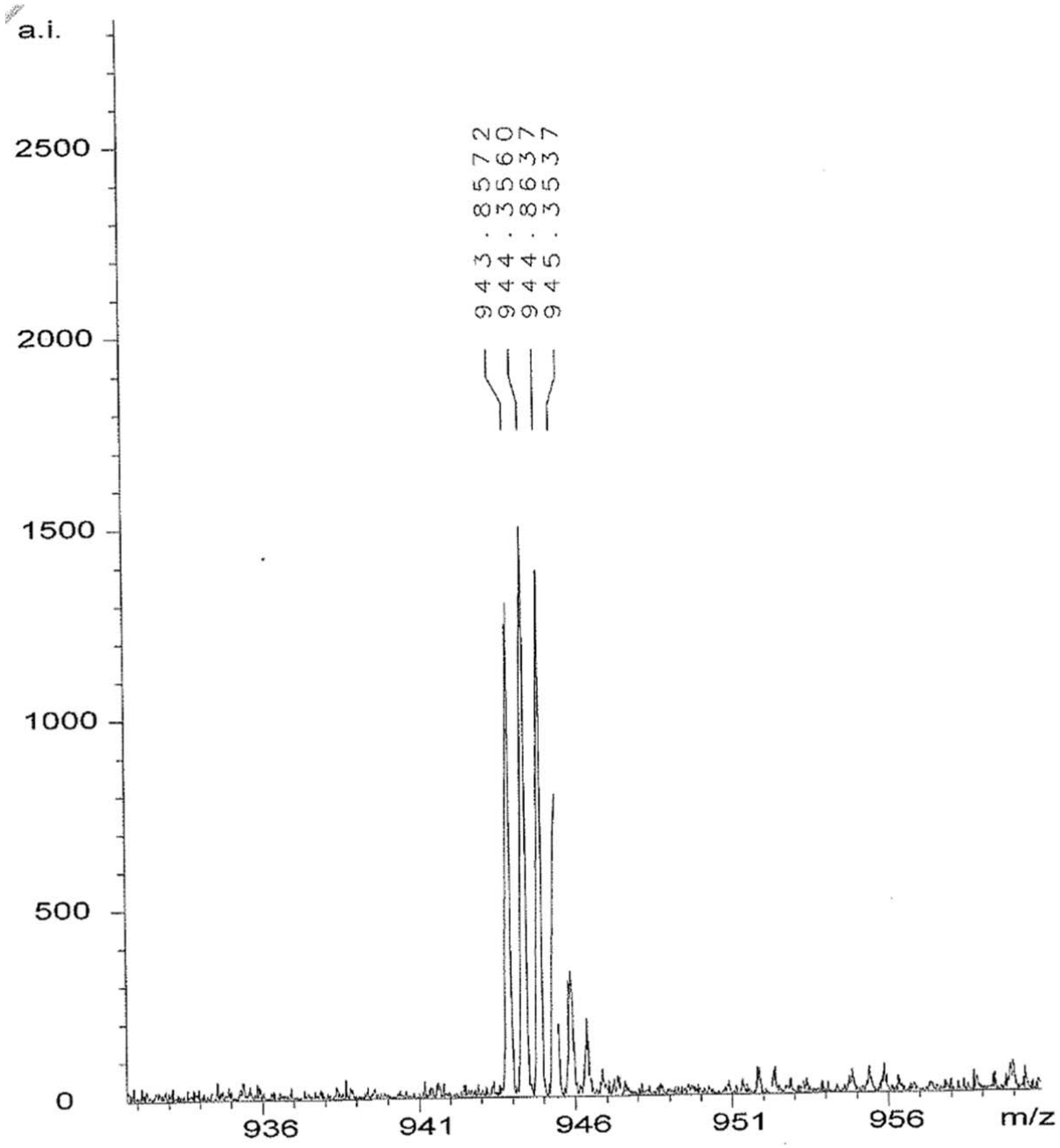

ESI-TOF mass spectra of KR12

ESI-TOF mass was produced on a BioTOF II (Bruker Daltonics) mass spectrometer using a positive ionization mode. ESI-TOF mass spectra indicated the [M+2H]2+ ions of KR12: calculated 1885.7027, observed 1885.6984

Supplementary Figure 9

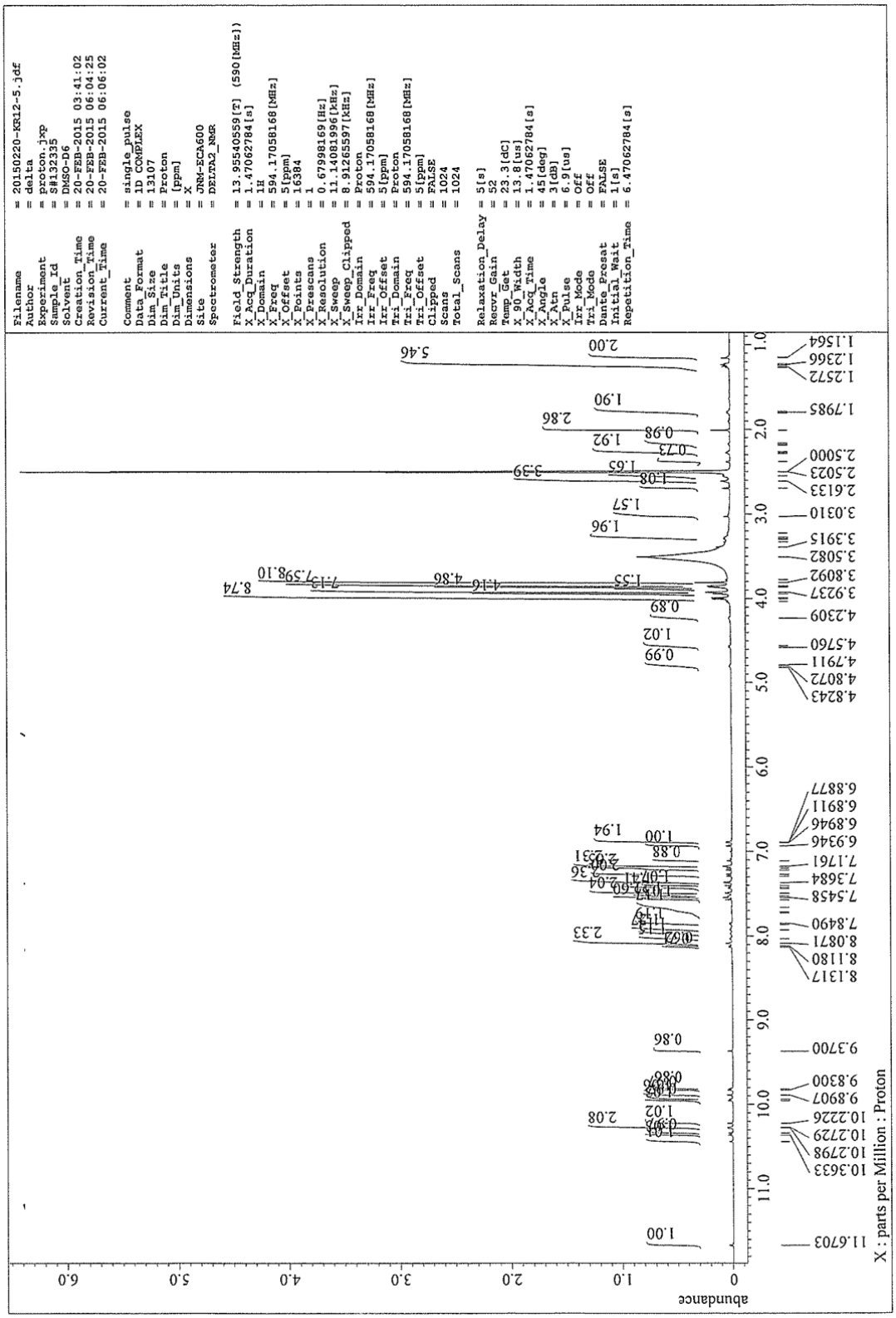

NMR spectra of KR12

1H NMR spectra was recorded with a JEOL JNM ECA-600 spectrometer operating at 600

MHz; the spectra were recorded in parts per million (ppm) downfield relative to tetramethylsilane used as an internal standard. The following abbreviations apply to spin multiplicity: s (singlet), d (doublet), t (triplet), q (quartet), m (multiplet).

^{1}H NMR (600 MHz, DMSO-d_6): δ = 11.67 (s, 1H), 10.44 (s, 1H), 10.36 (s, 1H), 10.34 (s, 1H), 10.28 (s, 1H), 10.27 (s, 1H), 10.22 (s, 1H), 9.95 (s, 1H), 9.94 (s, 1H), 9.89 (s, 1H), 9.83 (s, 1H), 9.82 (s, 1H), 9.37 (s, 1H), 8.12 (d, J = 8.2 Hz, 1H), 8.09 (brt, 2H), 8.03 (t, J = 5.5 Hz, 1H), 7.97 (brs, 1H), 7.93 (brt, 1H), 7.86 (d, J = 8.9 Hz, 1H), 7.57 (s, 1H), 7.55 (s, 2H), 7.53 (s, 1H), 7.50 (s, 1H), 7.49 (s, 1H), 7.43 (d, J = 8.9 Hz, 1H), 7.41 (s, 1H), 7.368 (s, 1H), 7.367 (t, J = 7.6 Hz, 1H), 7.29 (s, 1H), 7.27 (s, 1H), 7.22 (s, 1H), 7.20 (s, 1H), 7.18 (s, 2H), 7.11 (s, 1H), 6.93 (s, 1H), 6.89 (m, 2H), 4.81 (t, J = 10.0 Hz, 1H), 4.57 (d, J = 11.0 Hz, 1H), 4.23 (brt, 1H), 4.03 (m, 2H), 4.00 (s, 3H), 3.99 (s, 3H), 3.94 (s, 3H), 3.93 (s, 3H), 3.92 (s, 3H), 3.87 (s, 3H), 3.86 (s, 3H), 3.85 (s, 3H), 3.81 (s, 3H), 3.78 (s, 3H), 3.29 (m, 2H), 2.61 (m, 2H), 2.55 (m, 2H), 2.38 (m, 1H), 2.28 (t, J = 7.4 Hz, 2H), 2.18 (t, J = 7.9 Hz, 1H), 2.01 (s, 3H), 1.90 (m, 1H), 1.80 (apparent quintet, J = 6.9 Hz, 2H), 1.64 (m, 1H)

Supplementary Table 1. Summary table of the dissociation constants and BIACORE sensorgrams for each experiment.

PI-Polyamide	Sequence	KD(10^{-9} M)
KR12-Dp	WT(GGT)	114.0
	MUT(GAT)	8.5
	MUT(GTT)	17.1
#6-Dp	WT(GGT)	262.0
	MUT(GAT)	227.0
	MUT(GTT)	247.0

Dissociation equilibrium constants (KD) were calculated by fitting the resulting sensorgrams using a two-state reaction model. The KD values for KR12Dp with MUT (GAT) DNA and KR12Dp with MUT (GTT) DNA were calculated as 8.5×10^{-9} M and 1.71×10^{-8} M, respectively. Those KD values showed significantly higher binding affinity compared with the KD values for the mismatch binding, where the KD value for KR12Dp with WT (GGT) DNA was 1.14×10^{-7} M. However, the KD value for #6Dp with WT (GGT) DNA was identified as 2.62×10^{-7} M, that for #6Dp with MUT (GAT) DNA was 2.27×10^{-7} M, and that for #6Dp with MUT (GTT) DNA was 2.47×10^{-7} M. The KD values for mismatch binding were significantly lower than the KD values for full-match binding.

Supplementary Table 2. IC50 of KR12 in human colorectal cancer cell lines.

Cell lines	KRAS status	KRAS	P53 status	KR12 IC50(nM)	CBI IC50(nM)
SW480	MUT	G12V	MUT	31	10
SW620	MUT	G12V	MUT	17	10
SNU-C2B	MUT	G12D	MUT	57	18
LS180	MUT	G12D	WT	42	17
SW1463	MUT	G12C	MUT	178	20
DLD-1	MUT	G13D	MUT/WT	153	13
HT-29	WT	WT	MUT	102	25
Caco-2	WT	WT	MUT	105	18

Half maximal (50%) inhibitory concentration (IC50) values of KR12 and CBI in a series of colon cancer cell lines with a variety of KRAS mutations. Three independent experiments in

96-well plates using the MTT method were performed, as described in Fig. 2 (a). The KRAS and p53 mutation statuses of each cell line are indicated. Light grey-coloured columns indicate cell lines with KRAS mutations recognised by KR12.

Supplementary Table 3. Allele-specific expression, as shown by direct sequencing and colony PCR assays.

Compounds	Number of colonies (%)			
	colony sequence		colony PCR	
	WT	MUT	WT	MUT
DMSO	19 (50)	19 (50)	17 (61)	11 (39)
KR12	29 (67)	14 (33)	27 (73)	10 (27)
#6	15 (41)	22 (59)	14 (52)	13 (48)

*** $p < 0.05$**

Fifty ampicillin-resistant white colonies with subcloned inserts from cDNA of each treated cell type were randomly selected. Plasmid DNA was purified from these colonies and analysed by standard PCR using primer sets specific for wild-type *KRAS* or *KRAS* codon 12 mutant or by direct sequencing using the Sanger method for independent colony pick-ups. The numbers of colonies with wild-type (WT) or mutated (MUT) DNA sequences are indicated, with percentages in parentheses. Any colonies with ambiguous sequences were ignored in this study.

Supplementary Table 4. Establishment of human colorectal cancer xenograft models.

	Tumour doubling time (day)	SD	Median survival (day)	SD
HT29 (KRAS WT)	23.7	19	64	16.3
LS180 (12D/WT)	4.4	0.716	16.8	1.64
SW480 (12V/12V)	15.3	7.35	56.3	24.3

The eight human colorectal cancer cell lines used in this study were implanted into the right thighs of 6-week-old female mice. Three of the most appropriately and constantly inoculated cells (HT29, LS180 and SW480) were selected for this study, and five mice of each implantation group were tested for health status, body weight, tumour doubling time and median survival time. The table shows the tumour doubling time and median survival time,

with the standard deviation of each cell line xenograft model. All animals maintained a healthy status without weight loss during the experiments, but the tumour did not outgrow the right thigh.